THE JOURNAL OF PHYSICAL CHEMISTRY B

ARTICLE

pubs.acs.org/JPCB

Probing the Time Scale for Bulk Equilibration and Mass Transport of Water in Amorphous Inorganic Aerosol

Kai-Kai Li,[†] Feng Wang,[†] Guang Zeng,[†] Jonathan P. Reid,[‡] and Yun-Hong Zhang*[,†]

[†]The Institute for Chemical Physics, Key Laboratory of Cluster Science, Beijing Institute of Technology, Beijing 100081, People's Republic of China

[‡]School of Chemistry, University of Bristol, Bristol BS8 1TS, United Kingdom

ABSTRACT: New techniques are required to explore directly the kinetics of water transport in aerosol between the gas and condensed phases, both at high relative humidity (RH) close to saturation and at low RH where the role of amorphous states must be considered. Here, we present micro-Raman measurements of the kinetics of water transport between the bulk of a particle and the surrounding gas phase by examining the rate of exchange of D_2O by H_2O in droplets initially composed of $MgSO_4/D_2O$. The formation of an amorphous gel inhibits the response of the droplet composition to changes in the ambient RH and leads to a substantial reduction of the mass transfer rate of water in the droplet bulk with an apparent diffusion constant of 10^{-15} to 10^{-14} m^2 s^{-1}. These measurements are consistent with the imposition of a kinetic limitation on the time response of the aerosol particle size to changes in RH.

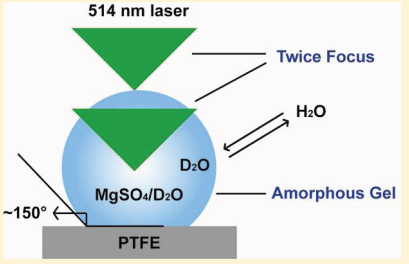

INTRODUCTION

Depending on their concentration and composition, aerosols can influence climate directly by absorbing and scattering incoming solar radiation and indirectly by acting as cloud condensation nuclei (CCN).[1,2] Interactions of atmospheric aerosols with water are critical in interpreting their optical properties and in determining their capacity to activate as CCN and become cloud droplets. Aerosol particles grow or contract through the condensation or evaporation of water vapor with variation in ambient relative humidity (RH), leading to an increase or decrease in optical cross-section.[3−5] Numerous investigations have focused on exploring the mechanism of evaporation, condensation, and water uptake by aerosol particles.[6−11] New techniques are required to interrogate directly the kinetics of water transport between the gas and condensed phases, both at high RH close to activation and at low RH where the role of amorphous states must be considered. For example, Miles et al. have recently explored the molecular uptake of water at RHs approaching saturation by resolving the kinetics of subnanometer size changes at the surface of an aqueous droplet.[12] In this article, we present a study of the mass transport in amorphous aerosol under dry conditions.

Although the deliquescence and efflorescence of inorganic aerosols and the change in water partitioning between the gas and solution phases with a change in RH have been studied extensively, the hygroscopic properties of mixed component inorganic/organic aerosols are much less well understood. In particular, organic and mixed component aerosols can show continual uptake or loss of water without the observation of discrete phase changes.[5,13,14] Amorphous phases can form at low RH, and such behavior has been seldom explored and difficult to characterize. Amorphous substances can be classified as glasses, rubbers, gels, or viscous liquids depending on their viscosity and microstructure, and their transition to a solution phase droplet may proceed through intermediate metastable states.[15] The absorption of water vapor into the bulk of particles can be kinetically limited either by surface processes, such as mass accommodation, or by diffusion into the particle bulk.[16] The high viscosity and low molecular diffusivity of water in amorphous phases can impose a kinetic limitation on water partitioning and a state of disequilibrium can persist for many hours.[17]

The unique properties of $MgSO_4$ aerosols have attracted much interest.[18] Chan and co-workers suggested that electrodynamic balance (EDB) observations of the mass of single $MgSO_4$ droplets were consistent with a significant increase in the diffusional resistance to water transport in the particle bulk during the response to changes in RH. They attributed the slow response in particle mass to the formation of a gel structure at low RH.[19] Zhang and Chan probed the intermolecular interactions between the inorganic ions and water in $MgSO_4$ droplets when in a supersaturated solution state using Raman spectroscopy coupled with an EDB. From the change in the Stokes shift for the Raman active vibrations of the sulfate ion, it was inferred that the gel state formed at low RHs is composed of polymeric chains of contact ion pairs (CIPs). It was suggested that the presence of polymeric CIP chains could inhibit the mass transfer of water within the particle bulk.[20] Wang et al. examined the formation of CIPs with decreasing RH for $MgSO_4$ droplets on a hydrophilic quartz substrate using confocal Raman spectroscopy. During a dehumidifying−humidifying cycle at low RH (<40%), the formation of the

Received: September 28, 2011
Revised: October 25, 2011
Published: October 26, 2011

chains of CIPs was observed to progress through a hysteresis: the appearance of chains of CIPs was delayed during drying and persisted during humidification.[21] In a subsequent publication, they observed a difference between the Raman spectra recorded from the near-surface region and the droplet center, suggesting inhomogeneity in water activity through the droplet bulk and the formation of a thin layer of a gel at the droplet surface.[22] However, it remains unclear how the gel structure influences the mass transfer kinetics of water between the gas and condensed phase.

In this article, we will report studies that probe the kinetics of water transport between the bulk of a particle and the surrounding gas phase by examining the rate of exchange of D_2O by H_2O in droplets initially composed of $MgSO_4/D_2O$. Measurements are made using confocal micro-Raman spectroscopy of a droplet supported by a hydrophobic Teflon substrate, ensuring that the droplet maintains an approximately spherical shape. The formation of an amorphous gel inhibits the response of the droplet size and composition to changes in the ambient relative humidity, and leads to compositional differences between the near-surface and droplet bulk. The confocal micro-Raman technique provides an appropriate approach for resolving the difference in the composition between the droplet bulk and the surface due to its high spatial resolution (3−4 μm in vertical). In particular, the radius of curvature of the droplet surface is considerably larger than that of the beam focus, and translating the image depth can allow depth profiling to be achieved and the diffusion of water in a mass transfer limited $MgSO_4$ gel to be monitored.

EXPERIMENTAL METHODS

Sample Preparation. Anhydrous $MgSO_4$ powder desiccated for more than two weeks was dissolved in D_2O. Using a microsyringe, $MgSO_4/D_2O$ droplets were deposited onto a hydrophobic polytetrafluoroethylene (PTFE) substrate. It was reported that a water droplet on PTFE has a contact angle of 150°.[23] Thus, we assume that the contact angle of an $MgSO_4$ droplet should be similar to or even more than 150° due to the large surface tension of the gel state, ensuring that the droplet maintains an approximately spherical shape. Dry N_2 gas was flushed through the sample chamber continuously to eliminate undeuterated water vapor. It can be assumed that the immediate exposure of droplets to a water activity of ~0 led to the rapid loss of water from the droplets and the formation of an amorphous aerosol, possibly with the formation of a compositional gradient within the particle.[15] The RH in the chamber was adjusted by changing the flux ratio of dry N_2 to water (H_2O) saturated N_2. The real-time RH was monitored by a humidity−temperature meter (Centertek Center310) with an accuracy of ±2.5% RH and ±0.7 °C. Spectra were recorded during the exchange of residual D_2O in the droplet by H_2O.

Apparatus for the Measurements. The experimental setup used in this study was described in detail in our previous work.[24] Briefly, the confocal Raman system (Renishaw InVia) equipped with a Leica DMLM microscope was used to acquire Raman spectra, and brightfield imaging was used to record morphological changes in the droplet state. The sample was excited by a 514.5 nm Ar ion laser with an output power of 20 mW. The inelastically backscattered signal from the droplet was collected by a spectrograph, dispersed by a 1800 g/mm grating, and detected by a charge-coupled device. Spectral calibration was made with respect to the 520 cm^{-1} Stokes shift silicon band prior to measurements. The spectral range was from 400 to 4000 cm^{-1} with a resolution of ~1 cm^{-1}, and spectra were acquired with a time-resolution of 1 s. All the measurements were made at an ambient temperature of 22−24 °C with a spectral reproducibility of 0.2 cm^{-1}, recorded by the Wire 2.0 program supplied by Renishaw. With a high confocal mode, the vertical resolution is 3−4 μm, and the horizon resolution is 1 μm. Considering the relatively large size of the droplet, the signature of the surface region can be distinguished from that of the bulk.

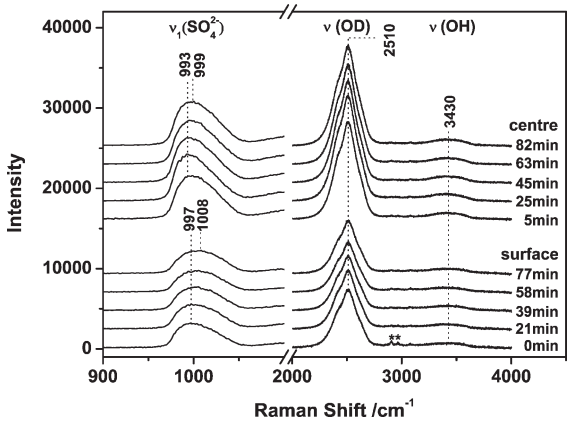

Figure 1. Raman spectra of the center and the surface of an $MgSO_4$ droplet (60 μm in diameter) as a function of time at a RH of <5%.

RESULTS AND DISCUSSION

Raman Spectra of the $MgSO_4/D_2O$ Droplets during Gel Formation. An $MgSO_4/D_2O$ droplet, with a diameter of ~60 μm, was deposited on the Teflon substrate under a flow of dry N_2 gas (with an RH of <5%). Figure 1 compares the Raman spectra of the $MgSO_4/D_2O$ droplet from the surface and center as a function of time. Over an evaporation time of 80 min, the ν_1-SO_4^{2-} band shifts from ~997 to ~1008 cm^{-1} when recorded from the surface. The spectra recorded at the center of the droplet show a blue shift in the ν_1-SO_4^{2-} peak from ~993 cm^{-1} to ~999 cm^{-1}. A small decrease is observed for the peak area of the O−D stretching band at ~2510 cm^{-1} at the surface of the droplet.

To reliably quantify and compare the degree of gel formation near the droplet surface and in the particle bulk, the shape of the ν_1-SO_4^{2-} band was resolved into three component bands at 983, 995, and 1021 cm^{-1}, and their relative weights estimated by nonlinear curve fitting. It is well-known that the ν_1-SO_4^{2-} band evolves in shape with the change in ion concentration. At the low Stokes shift side of the band around 983 cm^{-1}, the Raman signature is characteristic of free ions present in solution and can be attributed to the total contribution of pure hydrated ν_1-SO_4^{2-}, double solvent-separated (2SIP), and solvent-shared (SIP) ion pairs.[25,26] A component at 995 cm^{-1} has been assigned to contact ion pairs in many studies. With the combination of EDB and Raman, Zhang and Chan observed a shoulder appearing at 995 cm^{-1} in a supersaturated $MgSO_4$ droplet, which became the dominant peak at water-to-solute ratios (WSR) of less than 6. The frequency shift arises from the interaction of sulfate ions with Mg^{2+} ions with an incomplete hydration shell, i.e., monodentate contact ion pair.[20] This viewpoint is consistent with Rudolph et al. who attributed the appearance of a mode at 993 cm^{-1} in a $MgSO_4$ solution to the formation of an $MgOSO_3$ contact ion pair, an assignment that was confirmed by the observation

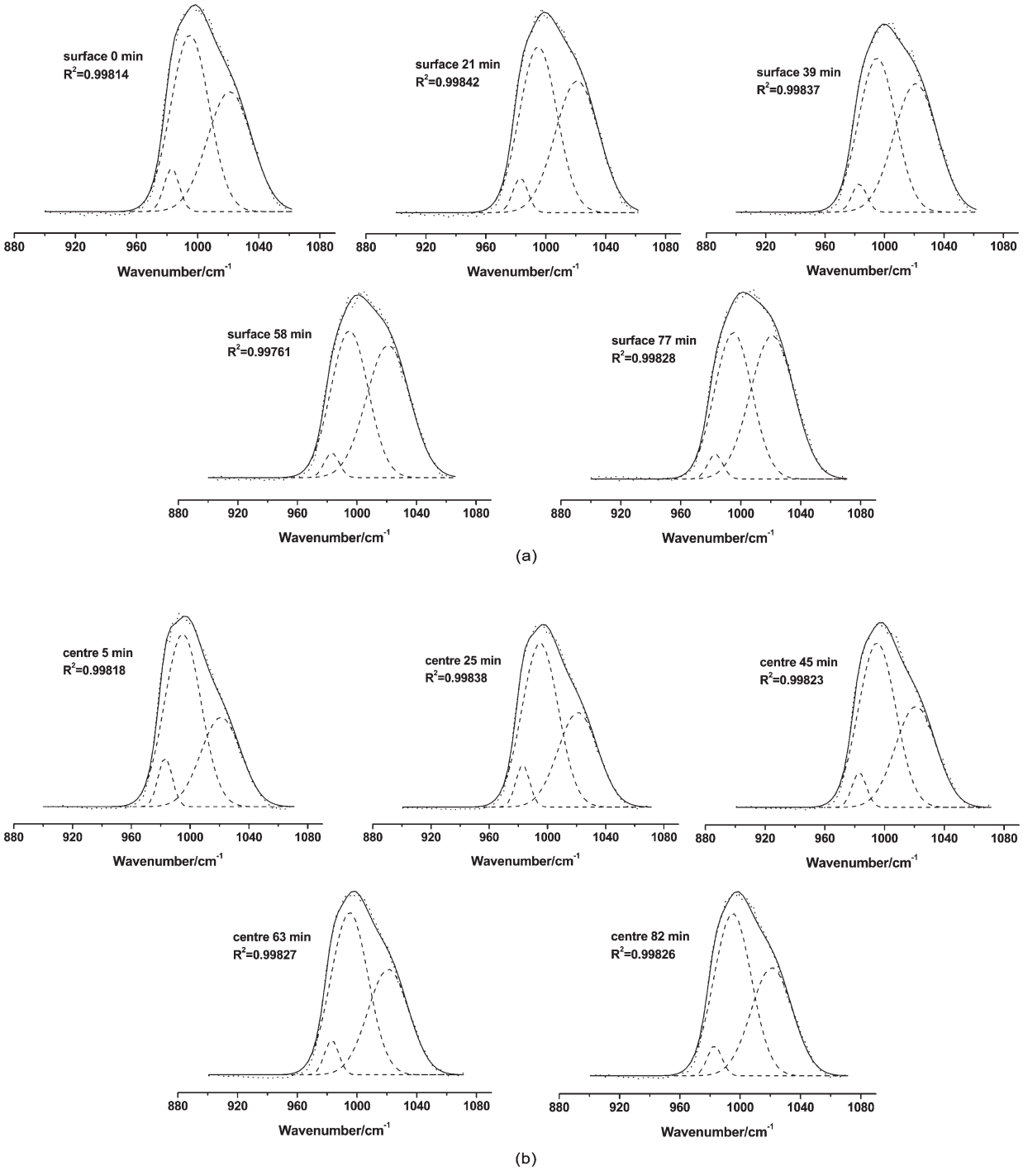

Figure 2. Experimental and fitted spectra in the region of 880−1080 cm^{-1} of the (a) surface and (b) center. Dotted lines: the experimental Raman spectra. Dashed lines: the three fitted spectral components. Solid lines: the sum spectra of the three fitted spectral components. R^2: the correlation coefficient.

of the stretching modes for the Mg−OSO_3 bond of the ligated SO_4^{2-} at 245 cm^{-1} and for the $(H_2O)_5MgOSO_3$ unit at 328 cm^{-1} in the Raman spectra.[25] In our previous work, Wang et al. observed hygroscopic properties of single $MgSO_4$ droplets on a quartz substrate. Under very dry conditions, a broad peak at 1021 cm^{-1} was attributed to a gel state formed from a bidentate chain structure.[21]Measurements were performed on a thin layer of liquid (∼1 μm thickness) on the quartz substrate, a thin enough layer that it can be assumed that equilibrium with the dry N_2 gas phase is always rapidly achieved. In this publication, the disequilibrium of the sphere droplet up to 60 μm in diameter can persist for many hours accompanied by the continuous shift of the ν_1-SO_4^{2-} band to higher shift Raman frequency up to 1008 cm^{-1}. This evolution can be attributed to the changing contributions of monodentate CIP at 995 cm^{-1} and the bidentate chain structure (gel state) at 1021 cm^{-1} with time.

The band deconvolution results are illustrated in Figure 2. All of the correlation coefficients are greater than 0.99. The band

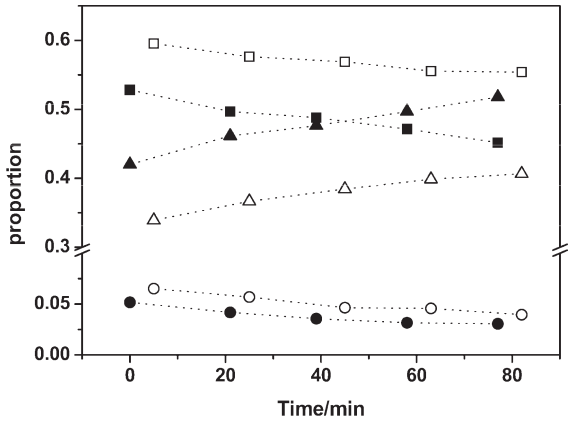

Figure 3. Proportions of the three fitted components in the $MgSO_4$ droplets at the surface (solid) and center (empty). Circles, squares, and triangles indicate free SO_4^{2-}, contact ion pair structures and gel state, respectively.

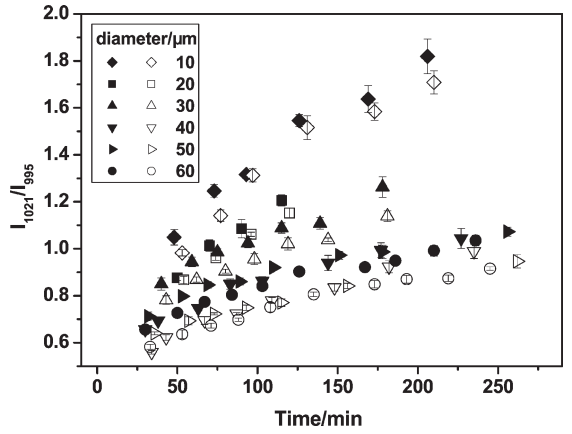

Figure 4. Gel degrees (I_{1021}/I_{995}) change with evaporation time at a RH of 5% at the surface (solid) and at the center (empty) for $MgSO_4$ droplets with different diameters between 10 and 60 μm.

located at 983 cm^{-1} and 995 cm^{-1} can be ascribed to free SO_4^{2-} ions and the contact ion pair structures, respectively.[20] The band appearing at 1021 cm^{-1} can be assigned to the gel state composed of chains of contact ion pairs.[21] Thus, the intensity ratio of I_{1021}/I_{995} can be used to characterize the extent of gel formation, i.e., the gel degree. The gel degree increases from 0.72 ± 0.01 to 0.91 ± 0.01 at the surface and from 0.63 ± 0.01 to 0.73 ± 0.01 at the center during the evaporation period. The immediate loss of D_2O from the droplet surface results in the rapid formation of a gel, consistent with the gel degree initially being larger at the droplet surface than in the particle bulk. At all times, the gel degree is lower at the center of the droplet, with mass transport of water from the center to the surface slowed by the gel formed at the surface. Thus, the delay in increase in the gel degree at the droplet center is a characteristic of gel formation at the surface and the slowing of water transport in the particle bulk.

The time-dependencies of the relative weights of the three components are illustrated in Figure 3. At a RH in the surrounding vapor of 5%, the component of free SO_4^{2-} ions decreases with time, and it accounts for the least proportion for both the surface and the center. For the center, the component of contact ion pairs stands for the largest proportion over 80 min, although it decreases from 0.60 to 0.55 with time accompanied by an increase in the component from the gel state from 0.34 to 0.41. For the surface, the proportion of contact ion pairs decreases from 0.53 to 0.45, while that of the gel state increases from 0.42 to 0.52 over 80 min. As a result, the component of contact ion pairs accounts for the largest proportion in the first 40 min. After that, the gel state becomes the dominant component. These data are consistent with the conversion of the contact ion pairs to the gel state and confirms that the gel starts to form at the surface with a delay of gel degree at the center.

Modeling the Influence of Gel Formation on the Mass Transport of Water in the Particle Bulk. In order to understand the evaporation kinetics leading to gel formation and the slowing of water transport in the particle bulk, the time dependence of the gel degree was examined under constant exposure to a dry N_2 gas flow for droplets in the size range from 10 to 60 μm in diameter (Figure 4). At any chosen time, the gel degree is higher for smaller droplets, consistent with a limitation imposed on the drying of the droplet by bulk diffusion. In addition, the measurements consistently show a delayed response in the gel degree at the droplet center, indicative of the increase in time scale required for water to diffuse through the droplet bulk and evaporate from the droplet surface. The time dependencies of the gel degrees at the droplet center will now be used to estimate the apparent diffusion coefficient of water in the gel phase.

The kinetics of water transport between the gas phase and amorphous gel can be described by a differential step isothermal method, the details of which can be found elsewhere.[27] Briefly, a simplified expression for the initial region of the uptake curve may be obtained as

$$\frac{m_t}{m_\infty} = \frac{\bar{q} - q_0}{q_\infty - q_0} \approx \frac{2S}{V}\sqrt{\frac{D_{ap}t}{\pi}} \quad (1)$$

where $\bar{q}$ is the average time-dependent water content in the sample, and m_t/m_∞ is the fractional approach to the sorption equilibrium. S/V is the ratio of the external surface area-to-particle volume and is $3/R_p$ for a spherical particle of radius R_p. D_{ap} is the apparent water diffusivity. The diffusivity depends on the pore diffusivity, D_e, the grain porosity, ε, and the shape of the water sorption isotherm with a slope of K.

As shown in Figure 5, m_t/m_∞ shows a linear dependence on $(t)^{0.5}/R_p$ with a slope $((3.5 \pm 0.5) \times 10^{-7}$ m^2 $s^{-1})$ that is consistent with eq 1 for droplets of different size, apart from for the very smallest diameter. The value of $\bar{q}$ is estimated from the area ratio of D_2O to SO_4^{2-} recorded in the droplet center, corresponding to the gel degrees in Figure 4. The value of q_0 is the initial area ratio, and q_∞ is estimated by performing a curve fitting to the dependence of area ratio on time to get the value of q at infinite time. From the gradient, the apparent diffusion constant (D_{ap}) can be estimated as $(1.1 \pm 0.3) \times 10^{-14}$ m^2 s^{-1}. Measurements of the gel degree at the surface are difficult to quantitatively interpret as the probe depth is ambiguous. It is shown in Table 1 that D_{ap} is in the range of 10^{-15} to 10^{-14} m^2 s^{-1} for all droplet sizes studied. For comparison, the reported experimental value of the diffusion constant for water diffusing in water is $\sim 2 \times 10^{-9}$ m^2 s^{-1},[28] and measurements of the diffusion constant of water in glassy sucrose aerosol have reported values of 10^{-16} to 10^{-19} m^2 s^{-1}.[17] The reported value of the water diffusion constant in radiation cross-linked polymer network hydrogels was 10^{-11} m^2 s^{-1}.[29] Thus, the formation of a gel clearly reduces the mass transfer rate of water between the gas and condensed phases.

dx.doi.org/10.1021/jp209379f |J. Phys. Chem. B 2011, 115, 14397–14403

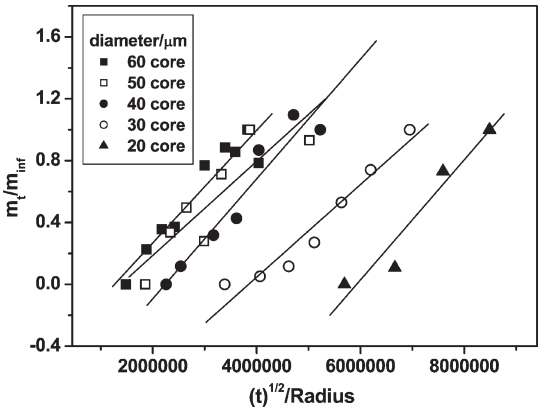

Figure 5. Plot of m_t/m_∞ versus $(t)^{0.5}/R_p$ for droplets with varying diameters. The slope of the linear fit curve represents the apparent diffusion constant of water.

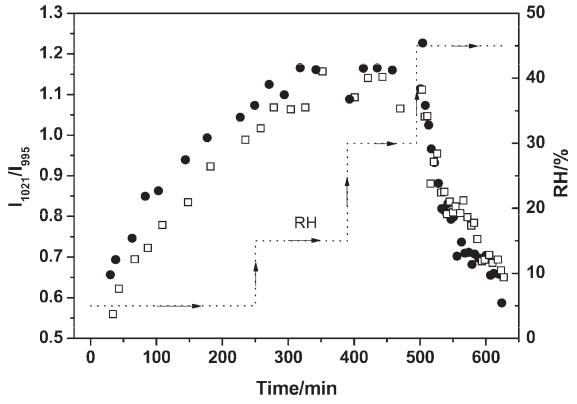

Figure 6. Gel degrees (I_{1021}/I_{995}) at the surface (solid circle) and at the center (empty square) of a $MgSO_4/H_2O$ droplet (40 μm in diameter) as a function of time at various RHs. The dotted line indicates the change route of RH.

Table 1. Slope of the Linear Fitting Curve, the Diffusion Constant, and the Porosity for Droplets with Varying Diameters

diameter (μm)	k	D (m^2 s^{-1})	ε
60	3.6×10^{-7}	1.2×10^{-14}	0.74
50	3.0×10^{-7}	8.1×10^{-15}	0.66
40	3.9×10^{-7}	1.3×10^{-14}	0.76
30	3.0×10^{-7}	7.8×10^{-15}	0.66
20	3.9×10^{-7}	1.3×10^{-14}	0.76

Gels are a two-phase mixture of a liquid dispersed in a (semi)solid amorphous matrix. Water can be considered to diffuse in the pores of the (semi)solid network. Thus, the porosity of the particle ε can also be estimated, with $D_{ap} = D_e/\varepsilon + (1 + \varepsilon)K$. The pore diffusivity D_e can be approximated as the diffusion constant of water in water. K depends on the local slope of the water sorption isotherm dq/dc, where q is the water concentration in the adsorbed phase, and c is the water concentration in the gas phase. Here, K is calculated according to the mass fraction of solute versus water activity data.[20] It is shown in Table 1 that depending on the diameter of the droplets, the upper and lower limits on the porosity ε are 0.76 and 0.66, respectively. The effective porosity is defined as the ratio of the total volume of interconnected pores in porous media to the total volume of the porous media, i.e., the porosity reflects the proportion of the pore volume to the total volume of the porous material. The water diffuses in the veins and pores in the particle bulk, which may be a network consisting of the chain structures formed by CIPs of Mg^{2+} and SO_4^{2-}. Despite the relatively large porosity of $MgSO_4$ gel, at the surface where the gel degree is high, the pores may be very narrow and lower in volume fraction than in the bulk. Thus, although we have reduced the kinetic interpretation to an idealized case of a particle consisting of uniform porosity throughout, it is likely that the porosity is considerably lower at the droplet surface than in the bulk due to the higher gel degree in the near surface region.

Dissociation of the Gel with an Increase in Relative Humidity. An $MgSO_4/D_2O$ droplet with a diameter of ~40 μm was prepared by flowing pure N_2 for 2 h (~5% RH). The RH was increased in steps of 10−15%. Notably, up to an RH of 30%, the gel degree increases even though the water activity is being increased, suggesting that the particle remains in a state of disequilibrium

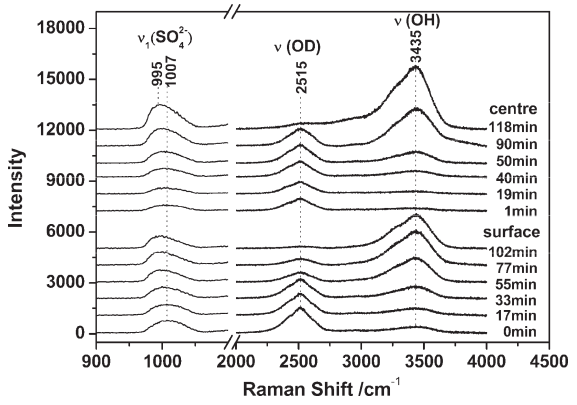

Figure 7. Raman spectra of the surface and the center of an $MgSO_4$ droplet (40 μm in diameter) as a function of time at RH of 45%.

throughout the measurement and is continually losing water even though the gas phase water activity is increasing. This is reminiscent of the hysteresis behavior observed by Wang et al.,[21] and the gel degree of the surface is in advance of the gel degree of the center. When the droplet is exposed to a dry N_2 gas, the rapid gel formation in the surface region will cause the center to retain an elevated water activity of about 0.4 due to the slowing of water transport. As a result, the particle continues to lose water, and the gel degree in the droplet center continues to increase even as the gas phase relative humidity is increased up to 30% RH. This is only reversed when the relative humidity is increased to 45% RH. Once an RH of ~45% is reached, the gel structure begins to dissociate, and the gel degree decreases rapidly, with the droplet surface and bulk finally having similar values (Figure 6). The gel begins to dissociate from the surface, and the bulk of the droplet persists with a higher gel degree for longer, consistent with a delayed response to the change in the gas phase water activity. As a result, the gel degree of the surface becomes less than the bulk, contrary to the situation before the RH is increased to 45%. Such observations are consistent with the temporary formation of core−shell structures with higher diffusivity in the outer shell, a consequence of water uptake beginning at the surface.[30]

The exchange between H_2O and D_2O during gel dissociation can be monitored from the in situ Raman spectra (Figure 7). The red shift of the ν_1-SO_4^{2-} band suggests the dissociation of gel

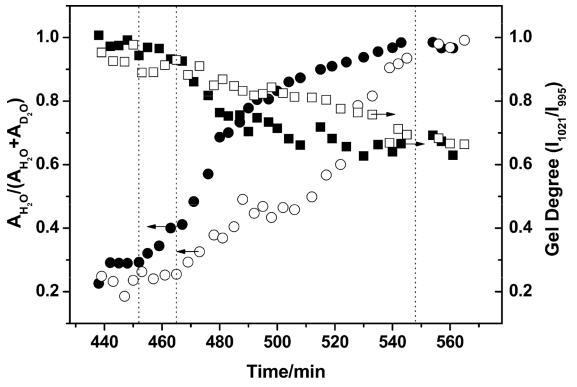

Figure 8. Gel degrees (square, right axis) and stretching band area ratios (circle, left axis) of water to the sum of water and heavy water at the surface (solid) and at the center (empty) of an $MgSO_4$ droplet (40 μm in diameter) as a function of time at RH of 45%.

state. During the first 30 min following the increase in RH to 45%, the area decrease of the O−D stretching band and the area increase of the O−H stretching band are very slow for both the surface and the center. At ∼33 min, the surface Raman spectra show that the area of the O−H stretching band is equal to that of the O−D stretching band. After ∼40 min, the area increase of the O−H band and the decrease of the O−D band become increasingly rapid. For the center, the O−H stretching band arrives at the same area of the O−D stretching band after ∼50 min, delayed by 17 min compared with that of the surface.

The time dependent gel degree and the stretching band area ratios of water to the sum of water and heavy water for the surface and the center are shown in Figure 8. The trends in gel degree and appearance of the H_2O signature are inversely correlated, with the two quantities changing more rapidly from early time when measured at the surface and with a more delayed response in the droplet center. This observation can be attributed to the uptake of H_2O as well as the evaporation of D_2O. The behavior can be divided into differing regimes at different times for the convenience of discussion, indicated by the dotted lines in Figure 8. The initial gel degrees at the surface and in the center are 1.01 and 0.94, respectively. The signature of the water from the surface almost remains constant before 452 min. After that, dissociation of the gel at the surface eliminates the barrier to water uptake, which leads to an increase in the rate of water uptake and results in the rapid increase of the proportion of H_2O. This observation can be attributed to the uptake of H_2O as well as the evaporation of D_2O. The appearance of H_2O at the center begins at ∼465 min, a delay of ∼15 min compared to the surface. Notably, the gel degree at the center remains larger than that of the surface after 465 min. After ∼554 min, the gel degrees at the surface and in the center become the same, indicating the facile diffusion of water within the particle after this time and suggesting the droplet transition from the amorphous phase to a liquid after complete gel dissociation. In this period, the H_2O proportion at the surface and in the center is the same, suggesting the final equilibration of the liquid and gas phases.

CONCLUSIONS

The formation of a gel structure in $MgSO_4$ droplets at low RHs results in a mass transfer limit on water partitioning between the bulk condensed and gas phases. With micro-Raman spectroscopy, the laser beam can be focused at the surface and the center of spherical droplets, and spectral information can be obtained. The formation of gel leads to a reduction of the diffusion coefficient of water in the bulk of the droplet with an apparent diffusion coefficient of 10^{-15} to10^{-14} m^2 s^{-1}, and the porosity of the particle can be estimated to be in the range 0.66 to 0.76. Once the RH is increased above 45%, the dissociation of the gel leads to rapid equilibration with the ambient RH at the droplet surface, although the appearance of H_2O in the droplet center remains delayed. These measurements suggest that the time scales for the equilibration of aerosol at low RH must be studied in greater detail, and the results are consistent with recent observations of the delayed response in the size of the aerosol existing in a glassy state.

AUTHOR INFORMATION

Corresponding Author

*Phone: 86-10-68912652. Fax: 86-10-6891 2652. E-mail: yhz@bit.edu.cn.

ACKNOWLEDGMENT

We acknowledge support from the NSFC (20933001, 20873006, and 20903036) and the EPSRC through the award of a Leadership Fellowship (to J.P.R.).

REFERENCES

(1) O'Dowd, C. D.; Smith, M. H.; Consterdine, I. E.; Lowe, J. A. *Atmos. Environ.* **1997**, *31*, 73–80.
(2) Murphy, D. M.; Anderson, J. R.; Quinn, P. K.; McInnes, L. M.; Brechtel, F. J.; Kreidenweis, S. M.; Middlebrook, A. M.; Posfai, M.; Thomson, D. S.; Buseck, P. R. *Nature* **1998**, *392*, 62–65.
(3) Carrico, C. M.; Kus, P.; Rood, M. J.; Quinn, P. K.; Bates, T. S. *J. Geophys. Res.* **2003**, *108*, 8650.
(4) Quinn, P. K.; Bates, T. S.; Baynard, T.; Clarke, A. D.; Onasch, T. B.; Wang, W.; Rood, M. J.; Andrews, E.; Allan, J.; Carrico, C. M.; Coffman, D.; Worsnop, D. *Geophys. Res. Lett.* **2005**, *32*, L22809.
(5) Zobrist, B.; Marcolli, C.; Pedernera, D. A.; Koop, T. *Atmos. Chem. Phys.* **2008**, *8*, 5221–5244.
(6) Sayer, R. M.; Horn, A. B. *Phys. Chem. Chem. Phys.* **2003**, *5*, 5229–5235.
(7) Finlayson-Pitts, B. J. *Chem. Rev.* **2003**, *103*, 4801–4822.
(8) Rossi, M. J. *Chem. Rev.* **2003**, *103*, 4823–4882.
(9) Laskin, A.; Wang, H.; Robertson, W. H.; Cowin, J. P.; Ezell, M. J.; Finlayson-Pitts, B. J. *J. Phys. Chem. A* **2006**, *110*, 10619–10627.
(10) Tolocka, M. P.; Saul, T. D.; Johnston, M. V. *J. Phys. Chem. A* **2004**, *108*, 2659–2665.
(11) Kolb, C. E.; Cox, R. A.; Abbatt, J.; Ammann, M.; Davis, E. J.; Donaldson, D. J.; Garrett, B. C.; George, C.; Griffiths, P. T.; Hanson, D. R.; Kulmala, M.; McFiggans, G.; Poschl, U.; Riipinen, I.; Rossi, M. J.; Rudich, Y.; Wagner, P. E.; Winkler, P. M.; Worsnop, D. R.; O'Dowd, C. D. *Atmos. Chem. Phys.* **2010**, *10*, 10561–10605.
(12) Miles, R.; Knox, K. J.; Reid, J. P.; Laurain, A.; Mitchem, L. *Phys. Rev. Lett.* **2010**, *105*, 116101.
(13) Murray, B. J. *Atmos. Chem. Phys.* **2008**, *8*, 5423–5433.
(14) Bodsworth, A.; Zobrist, B.; Bertram, A. K. *Phys. Chem. Chem. Phys.* **2010**, *12*, 12259–12266.
(15) Mikhailov, E.; Vlasenko, S.; Martin, S. T.; Koop, T.; Poschl, U. *Atmos. Chem. Phys.* **2009**, *9*, 9491–9522.
(16) Poschl, U.; Rudich, Y.; Ammann, M. *Atmos. Chem. Phys.* **2007**, *7*, 5989–6023.
(17) Tong, H. J.; Reid, J. P.; Bones, D. L.; Luo, B. P.; Krieger, U. K. *Atmos. Chem. Phys.* **2011**, *11*, 4739–4754.
(18) Tang, I. N.; Tridico, A. C.; Fung, K. H. *J. Geophys. Res.* **1997**, *102*, 23269–23275.

(19) Chan, C. K.; Flagan, R. C.; Seinfeld, J. H. *J. Am. Ceram. Soc.* **1998**, *81*, 646–648.
(20) Zhang, Y. H.; Chan, C. K. *J. Phys. Chem. A* **2000**, *104*, 9191–9196.
(21) Wang, F.; Zhang, Y. H.; Li, S. H.; Wang, L. Y.; Zhao, L. J. *Anal. Chem.* **2005**, *77*, 7148–7155.
(22) Wang, F.; Shou, J. J.; Zhang, Y. H. *Chin. Sci. Bull.* **2008**, *53*, 2414–2416.
(23) Hiratsuka, K.; Bohno, A.; Endo, H. *J. Phys.: Conf. Ser.* **2007**, *89*, 012012.
(24) Li, X. H.; Zhao, L. J.; Dong, J. L.; Xiao, H. S.; Zhang, Y. H. *J. Phys. Chem. B* **2008**, *112*, 5032–5038.
(25) Rudolph, W. W.; Irmer, G.; Hefter, G. T. *Phys. Chem. Chem. Phys.* **2003**, *5*, 5253–5261.
(26) Buchner, R.; Chen, T.; Hefter, G. *J. Phys. Chem. B* **2004**, *108*, 2365–2375.
(27) Aristov, Y. I.; Glaznev, I. S.; Freni, A.; Restuccia, G. *Chem. Eng. Sci.* **2006**, *61*, 1453–1458.
(28) Guevara-Carrion, G.; Vrabec, J.; Hasse, H. *J. Chem. Phys.* **2011**, *134*, 074508.
(29) Hill, D. J. T.; Whittaker, A. K.; Zainuddin. *Radiat. Phys. Chem.* **2011**, *80*, 213–218.
(30) Zobrist, B.; Soonsin, V.; Luo, B. P.; Krieger, U. K.; Marcolli, C.; Peter, T.; Koop, T. *Phys. Chem. Chem. Phys.* **2011**, *13*, 3514–3526.